

The 2025 release of CLOUDY

Chamani M. Gunasekera ©¹, Peter A. M. van Hoof ©², Maryam Dehghanian ©³, Priyanka Chakraborty ©⁴,⁵, Gargi Shaw ©⁶, Stefano Bianchi ©⁷, Marios Chatzikos ©³, Masahiro Tsujimoto ©⁶ and Gary J. Ferland ©³

Keywords: Atomic data, Astronomy software, Active galaxies, Computational methods, Galaxy clusters, Molecular data

Abstract

We present the 2025 release of the spectral synthesis code CLOUDY, highlighting the significant enhancements in the scope and accuracy of the physics that have been made since the previous release. This key development resolves the Lyman α line into j-resolved fine-structure doublets, thereby making CLOUDY useful to the X-ray community. We also updated the inner-shell ionization line energies and incorporated the 1 keV feature that is commonly observed in X-ray binaries. In addition, we updated the Stout database for the carbon isoelectronic sequence, improving the CLOUDY microphysical calculations for all wavelengths. The molecular network has also been extended with new silicon-bearing species, titanium-related reactions, and phosphorus-containing molecules, enhancing CLOUDY's ability to model the complex chemistry relevant to exoplanet atmospheres. Finally, we outline future developments aimed at maximizing scientific returns from current and upcoming generations of observatories.

Resumen

Presentamos la versión 2025 del código de síntesis espectral CLOUDY, destacando las mejoras significativas en el alcance y la precisión de la física que se han realizado desde la versión anterior. El desarrollo clave resuelve la línea Lyman α en j dobletes de estructura fina resueltos, lo que hace que CLOUDY sea útil para la comunidad de rayos-X. También hemos actualizado las energías de la línea de ionización de la capa interna e incorporado la característica de 1 keV que se observa comúnmente en estrellas binarias de rayos-X. Además, actualizamos la base de datos Stout para la secuencia isoelectrónica del carbono, mejorando así los cálculos microfísicos de CLOUDY para todas las longitudes de onda. La red molecular también se ha ampliado con nuevas especies que contienen silicio, reacciones relacionadas con el titanio y moléculas que contienen fósforo, lo que mejora la capacidad de CLOUDY para modelar la compleja química relevante para el campo de las atmósferas de exoplanetas. Finalmente, describimos los desarrollos futuros destinados a maximizar el rendimiento científico de la generación actual y futura de observatorios.

Corresponding author: Chamani M. Gunasekera E-mail address: cgunasekera@stsci.edu Received: August 1, 2025 Accepted: October 12, 2025

1. Introduction

We introduce the next major release of CLOUDY, C25.00. CLOUDY is a spectral synthesis code, simulating plasma conditions ranging from highly non-equilibrium conditions to full Local and Strict Thermodynamic Equillibrium (LTE & STE). Beginning from the first principles of physics and chemistry, CLOUDY self-consistently solves the chemistry, radiation transport, and dynamics to determine the ionization, chemical state, temperature, and excitation of all species. Much of the physics is discussed in Osterbrock & Ferland (2006). It does so for the entire electromagnetic spectrum.

Ongoing development since 1978 has continually expanded the range of capabilities of the code. Table 1 lists previous review papers that captured the state of the code at that time. The last major release was C23.01 (Chatzikos et al., 2023; Gunasekera et al., 2023b). With each release, we aim to provide users with a tool that maximizes the impact of their research.

A major effort has been undertaken since C23.01, with the goal of enabling maximum science through the full suite of advanced observatories that are currently available. As detailed in § 4, the major development in this release was an update of CLOUDY'S H-like iso-sequence to match the spectral resolution of the X-

¹Space Telescope Science Institute, Baltimore, MD, USA.

²Royal Observatory of Belgium, Ringlaan 3, B-1180 Brussels, Belgium.

³Physics & Astronomy, University of Kentucky, Lexington, Kentucky, USA.

⁴Center for Astrophysics | Harvard & Smithsonian, Cambridge, MA, USA.

⁵University of Arkansas, Physics and Astronomy, 825 W Dickson St, Fayetteville, Arkansas 72701, USA.

⁶Department of Astronomy and Astrophysics, Tata Institute of Fundamental Research, Mumbai 400005, India.

⁷Dipartimento di Matematica e Fisica, Università degli Studi Roma Tre, via della Vasca Navale 84, 00146 Roma, Italy.

⁸ Institute of Space and Astronautical Science (ISAS), Japan Aerospace Exploration Agency (JAXA), 3-1-1 Yoshinodai, Chuo-ku, Sagamihara, Kanagawa 252-5210, Japan.

Table 1.	Major CLOUDY	release papers	
3.7		G:1 1:	

Version	Year	Citation
C33 - 87	1983 – 1998	Ferland (1991, 1993, 1996)+
C90	1998	Ferland et al. (1998)
C13	2013	Ferland et al. (2013)
C17	2017	Ferland et al. (2017)
C23, C23.01	2023	Chatzikos et al. (2023), Gunasekera et al. (2023b)

Ray Imaging and Spectroscopy Mission (XRISM). Additionally, in § 3 we present updates to our chemistry network to better equip CLOUDY for modeling the complex chemistry characteristics of the rapidly growing field of exoplanet atmosphere. We also present new updates to our atomic data in § 2, which allows for more accurate state-of-the-art microphysical calculations and improves the spectral predictions across the full electromagnetic range. Finally, § 5 and § 6 introduce new commands and data files designed to enhance usability for CLOUDY users. In light of these major developments, we strongly recommend that users upgrade to the latest version of CLOUDY, C25.00, which includes bug fixes that enhance the accuracy of the synthesized spectra and improve the overall usability.

2. Atomic Data

2.1. Stout

We have significantly extended the atomic database for the C-like isoelectronic sequence in CLOUDY by incorporating a new and comprehensive dataset. The updated dataset includes 590 fine-structure levels per ion, combining high-precision theoretical energies from R-matrix calculations (Del Zanna et al., 2025) with experimentally measured energies from the NIST Atomic Spectra Database Version 5.12 (Kramida et al., 2024). This expansion includes N II to Kr XXXI (i.e., N+ to Kr³0+) and enables a more accurate and complete treatment of excitation and emission processes in photoionized and collisionally excited plasmas. Further details are provided in a forthcoming paper (Dehghanian et al., in preparation). Note that the current workflows do not exercise species heavier than zinc, but we are completing their entries to ensure consistency and to enable future use.

It is worth mentioning that this release exhibits a longer startup phase, driven by the initialization of the enlarged STOUT database (the code currently scans and parses the full-text dataset at launch). Once the initialization is complete, the model execution is comparable to previous versions. We are actively working on a new solution to shorten startup times in future releases.

2.1.1. Energy levels

The theoretical energies are now enclosed in square brackets (e.g., [12345.6]) to distinguish between the experimental and theoretical values in the energy-level files. CLOUDY's internal parser has been enhanced to interpret this syntax, automatically flagging such levels as theoretical. This distinction is propagated throughout the simulation by adding a question mark after the wavelength unit where is appropriate in the .out file produced by the simulations. Figure 1 shows an example from a CLOUDY .out file, where the new feature, that is, the uncertain wavelengths derived from theoretical energy levels, is marked with a question mark.

```
0
  3
           5005.93A?
                        -8.714
                                 17.4419
0
  3
           5006.19A?
                        -9.581
                                  2.3652
0
  3
           5006.33A?
                        -8.964
                                  9 7965
           5006.84A
                        -5.809 13994.061
0
  3
           5006.88A?
                        -2.166 ******
0 3
           5006.89A
                        -6.589 2323.5645
```

Figure 1. Intrinsic line intensities from a sample CLOUDY model.

2.1.2. Transition probabilities

We updated the transition probabilities to align with the new energy-level structure. Dipole-allowed transitions are drawn from recent 2025 R-matrix calculations (Del Zanna et al., 2025), providing agreement with the corresponding collision strengths across 590 levels per ion. For forbidden lines, we retained the 2020 data (Mao et al., 2020) because they are not available in the 2025 version of the R-matrix calculations by Del Zanna et al. (2025). When the experimental energies from NIST were adopted, the associated NIST transition probabilities were used where available to maintain consistency. This hybrid approach ensures that TP data are physically self-consistent by combining modern theory with reliable measurements.

2.1.3. Collisional strengths

We also updated CLOUDY'S .coll files in the Stout directory for C-like ions using the recent R-matrix calculations from Del Zanna et al. (2025), which provides improved electron-impact collision strength across 590 levels per ion. These data agree with the updated energy levels and transition probabilities, ensuring accurate modeling of collisional excitation processes.

Special case of N II For N II, although we updated the Stout dataset in the same manner as for other ions in the isoelectronic sequence, CLOUDY defaults to using the CHIANTI dataset because it is based on a targeted study of singly ionized nitrogen (Tayal, 2011). The dataset included 58 energy levels. If the user prefers to use the Stout dataset (which includes 590 levels), they can simply enable it in the file data/stout/masterlist/Stout.ini.

Special case of O III In our modeling, we adopted a hybrid approach for [OIII] collision strengths, selecting the most reliable dataset for each set of transitions based on consistency, temperature coverage, and agreement across recent calculations. For transitions among the five lowest levels of O III we use the data from Storey et al. (2014) for $T_{\rm e} \leq 30,000$ K and then switch to Del Zanna et al. (2025) at higher temperatures. These include the important ground-term fine-structure lines at 88.35 μ m (1–2) and 51.81 μ m (2–3), as well as optical nebular lines, such as 5006.84 Å (3–4). For all other transitions involving higher excited levels

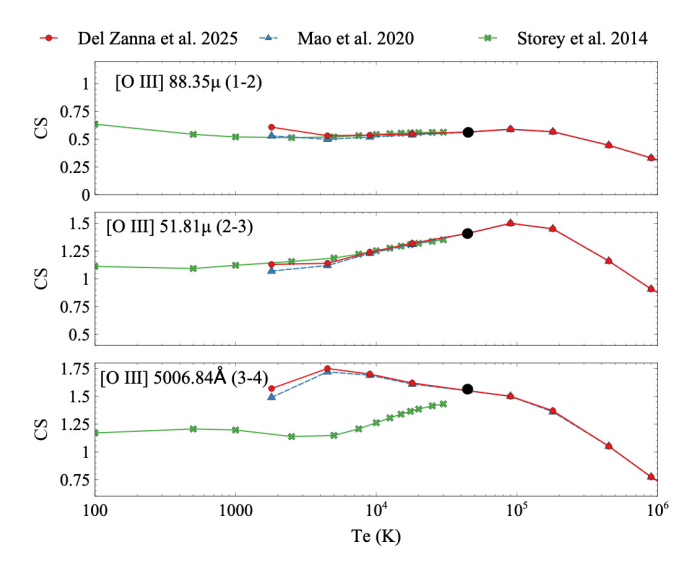


Figure 2. Temperature-dependent thermally-averaged CS for four key [O III] transitions, showing differences in the 88.35 μ m and 5006.84 Å lines at $T_e < 10^4$ K. These discrepancies motivated the adoption of a hybrid dataset for transitions among the five lowest levels. The black dot on the plots marks this threshold temperature, indicating the point at which we change the reference dataset for the lower levels.

beyond the lowest five, we adopted more recent data from Del Zanna et al. (2025). This dataset, which builds upon and corrects the earlier Mao et al. (2020) results, is based on a systematic Rmatrix calculation across the entire carbon isoelectronic sequence. The Del Zanna dataset resolves previous inconsistencies and includes a critical bug fix that affects the earlier values. While Del Zanna et al. (2025) show strong agreement with Storey et al. (2014) for many transitions, noticeable differences remain - especially for transitions involving level 4, such as 3-4 primarily at lower temperatures relevant to photoionized plasmas. Given that photoionized clouds can extend to temperatures below 10⁴ K, where such discrepancies significantly impact emissivity predictions and derived abundances, our hybrid strategy ensures both consistency with widely used references and the incorporation of the most accurate atomic data available for the full temperature range of interest.

Figure 2 compares the temperature-dependent collision strengths (CS) for the three key [O III] transitions using data from three sources. The red curves show the updated values from Del Zanna et al. (2025), the blue dashed curves represent the earlier results from Mao et al. (2020), and the green curves show the values from Storey et al. (2014), which are currently adopted in CLOUDY version C23.01. For the 51.81 μ m (2-3) transition, all three datasets are in excellent agreement across the entire temperature range. In the case of the 88.35 μ m (1–2) and 4363.21 Å (4-5) lines, small discrepancies were observed, with Storey et al. (2014) values being slightly lower than the others at low temperatures. However, the most significant deviation appears in the 5006.84 Å (3-4) transition, where both Mao et al. and Del Zanna et al. datasets overestimate the collision strength relative to the Storey et al. dataset, particularly at photoionization temperatures below 10⁴ K. In all three cases, the black dot indicates the temperature at which we switch to Del Zanna et al. (2025) from Storey et al. (2014).

Special case of Fe XXI While we extended the energy levels to 590 for all C-like isoelectronic ions, we were able to expand the

model for Fe XXI to include 620 levels by adding 30 levels with a K-shell vacancy. For this ion, levels 591-620 and the associated transition probabilities were extracted from Palmeri et al. (2003).

The new atomic structure framework improves CLOUDY's predictive power for diagnostic lines in C-like ions across UV and X-ray wavelengths and supports the demands of modern high-resolution instruments, such as the JWST and XRISM. We are actively working on extending this framework to additional isoelectronic sequences, with the goal of building a consistently high-fidelity atomic database for use in modern astrophysical modeling.

To illustrate the impact of the new atomic data on model predictions, Figure 3 (taken from Dehghanian et al., in preparation) compares the emission spectra of O III (upper panel) and Fe XXI (lower panel) generated using the previous dataset available in C23.01 (red crosses) and the newly updated dataset (gray dots) based on the C-like model described above. The updated model produces a substantially larger number of emission lines, particularly in the infrared region, and provides more physically complete predictions. This improvement enables more robust comparisons with high-resolution observations from facilities such as the JWST and XRISM. The denser distribution of lines also highlights the role of weak transitions that were previously missing or underestimated in the literature. Dehghanian et al. (in preparation), will provide a comprehensive review of these updates and details the implementation process.

2.2. Chianti Atomic Database

The Chianti atomic database used by CLOUDY has been updated to the newer version, Chianti v10.1 (Dere et al., 1997, 2023). Gunasekera et al. (2022a) introduced a script https://gitlab .nublado.org/cloudy/arrack that re-casts the latest Chianti database into the format used in Chianti v7 (Landi et al., 2012), which is the format compatible with CLOUDY. In the previous release of CLOUDY, we included a version of the Chianti database that contained only energy levels below the ionization potential, thereby excluding autoionizing levels. A complete version of the CLOUDY compatible Chianti v10.0 data (Del Zanna et al., 2021), including these autoionizing levels, was available separately on https://data.nublado.org/. With the current update, CLOUDY now includes Chianti v10.1 with all levels fully integrated (including autoionizing levels). This expanded dataset is particularly important for X-ray astronomy applications. The full database, as well as the version without autoionizing levels, of the CLOUDYcompatible Chianti v10.1 is available for download at https: //data.nublado.org/chianti/.

2.3. Updated H-like 2s Energies

During the work described in Gunasekera et al. (2024) to resolve the $2p_{1/2,3/2} \rightarrow 1s_{1/2}$ doublet (hereafter Lyman $\alpha_{2,1}$), the Ly α_2 line was found to overlap ambiguously with the $2s_{1/2} \rightarrow 1s_{1/2}$ M1 transition. This ambiguity arises because the upper levels of these transitions, 2p ($^2P_{1/2}$) and 2s, are closely spaced in energy. To disambiguate these lines, we updated the energy of the 2s levels of the H-like species to more accurate values obtained from Yerokhin & Shabaev (2015), thus clearly distinguishing M1 and the Ly α_2 lines.

2.4. Levels in Atomic Models

Because H-like Fe Ly α lines are important X-ray diagnostics, we increased the number of resolved levels included in the H-like

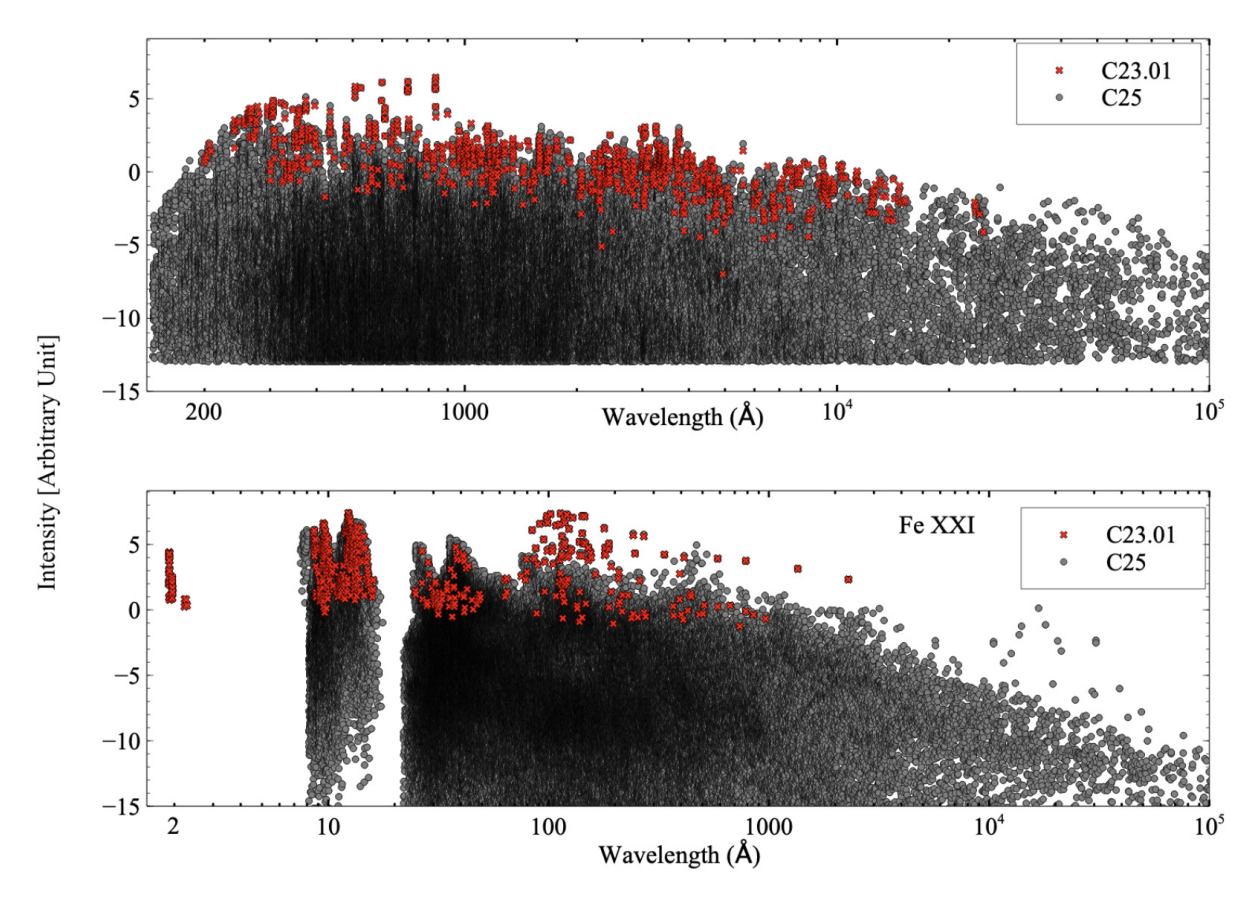


Figure 3. Comparison of predicted emission lines for O III (top) and Fe XXI (bottom) using the previous (C23.01, red) and updated (C25, gray) atomic datasets in CLOUDY (taken from Dehghanian et al., in preparation). The expanded and more complete atomic model used in the updated dataset results in a denser and more accurate distribution of predicted lines.

Fe XXVI atom by default from 15 to 55 (i.e., all nl-resolved levels up to n=10). Increasing the number of levels enables a more refined computation of the collisional physics occurring at higher energy levels. However, the size of the atomic models is restricted by the computing time and available memory.

Additionally, the number of collapsed levels of CVI, NVII, OVIII, SiXIV, and FeXXVI increased from 5 to 15. The number of collapsed levels is relatively computationally inexpensive because they are only *n*-resolved. Therefore, we increased the number of collapsed ions that contribute to a large fraction of the gas physics.

2.5. Improvements to the output

2.5.1. Main output

As a result of the work described in § 4.1, for lines whose energy separation is greater than a given spectral resolution (the default value for this resolution is 0.25 eV), CLOUDY now prints the j-resolved doublets, instead of the previous single line, under emergent and intrinsic line intensities.

2.5.2. 'save line labels' command

The code has been changed to provide the correct level indices in the save line labels output, as defined in the input files for the database. In previous versions, it provided the level indices as they were stored in memory after reading the data files. In principle, this change can affect all databases; however, in practice, this is only relevant for Chianti model atoms. This change also affects the level indices used for line disambiguation.

Additionally, the "extra" Lyman lines now have two entries in the save line labels output, one coming from the j = 1/2 line

stack and the other from j=3/2. The purpose of these lines is to fill in the "gaps" between the highest level and the continuum above, which arise owing to the nature of having a finite H⁰ model (also detailed in Section 3.1.4 of Ferland et al., 2017). Therefore, no changes were required in their treatment.

2.5.3. Line Labels

With the need to distinguish, for example, M1 lines from Ly α lines, or various line components from the main emission line, there arose a need for more verbose line labels. Therefore, the line labels in CLOUDY have been updated to use labels longer than our traditional use of four characters. However, these longer labels need to be in double quotes, for example, "Fe 26 M1". Previously, we had line components that contributed to the lines with the following labels:

- "Inwd"—fraction of the line re-emitted toward the source,
- "Pump"—contribution to the total line intensity by continuum pumping,
- "Coll"—contribution to the total line intensity by collisional excitations i.e. the contribution to the gas cooling by this line,
- "Heat"—contribution to the gas heating by this line by collisional de-excitation of the upper level (this is a negative contribution to the line intensity).

All species used the same labels. This made it difficult to identify the line to which the component contributed. We have now disambiguated this by expanding the labels to read, for example, "H 1 M1 Pump", replacing the previous "Pump M1".

3. Molecular Data

3.1. Temperature limits in UMIST chemistry

CLOUDY primarily uses reaction rate coefficients from the UMIST Database for Astrochemistry (UDfA) (Millar et al., 2024). In UDfA, the rate coefficient for a two-body gas-phase reaction is given by a modified Arrhenius-type formula:

$$k = \alpha \left(\frac{T}{300}\right)^{\beta} \exp(-\gamma/T),\tag{1}$$

where T is the temperature of the gas. The UDfA provides fitted coefficients that are valid for specific temperature ranges. However, CLOUDY operates across a much broader range of temperatures-from the cosmic microwave background (CMB) up to 10¹⁰ K, depending on the astrophysical environment. As a result, simply extrapolating these rate coefficients beyond their valid ranges can lead to unphysical values at both high and low temperatures. To prevent this, CLOUDY applies the following temperature caps: Following Shaw et al. (2023a), for $\beta > 0$, the rate is capped at high temperatures: k(T > 5000 K) = k(T =5000 K). For β < 0, the rate is capped at low temperatures: k(T <10 K) = k(T = 10 K). Similarly, for $\gamma < 0$, the rate is also capped at low temperatures to avoid divergence: k(T < 10 K) = k(T =10 K) (Röllig, 2011). These caps ensure the stability and physical plausibility of reaction rates over the wide range of temperatures modeled in CLOUDY.

3.2. Si-chemistry

We have extended our existing silicon-chemistry network (Shaw et al., 2022, 2023b), which now includes 21 Si-bearing species: SiS, HSiS, HSiS⁺, SiS⁺, SiC, SiC⁺, SiC⁺, SiNC⁺, SiH₂, SiCH₂, SiCH₂, SiCH₂, SiNC, SiN, SiN⁺, SiO⁺, SiC₂, SiH⁺₂, SiH, SiOH⁺, SiO, and SiO⁺. Notably, the reaction N + SiC⁺ \rightarrow Si⁺ + CN significantly affects the column density and line intensity of CN. Among these 21 Si-bearing molecules, line intensities were predicted for SiS, SiO, and SiC₂. The corresponding energy levels and collisional rate coefficients for these molecules are adopted from the LAMDA Database (Schöier et al., 2005).

3.3. Ti-chemistry and TiO

TiO is the dominant source of opacity in the atmosphere of cool stars (Lodders, 2002), and it is observed in the stellar atmosphere of M-type giant stars (Kamiński et al., 2013) as well. However, this is not observed in the ISM due to the high depletion of Ti. In environments devoid of dust, TiO is observed in the gas phase. Recently, we added 229 Ti-related reactions to the chemical network (Shaw et al., 2024). However, there is a scarcity of reaction rates for Ti chemistry. Hence, we have incorporated some reactions that are available in the UDfA (Tsai et al., 2021; Churchwell et al., 1980). For reactions that were not directly available, we scaled analogous silicon-based reactions from UDfA. In addition, we consider 230 fine-structure energy levels, the corresponding 223 radiative transitions, and 444 collisional transitions with ortho and para $\rm H_2$ and predicted 66 TiO lines. Further details are available in Shaw et al. (2024).

We modeled the circumstellar envelope of the oxygen-rich red supergiant VY Canis Majoris to validate our updates. Our model reproduced the observed column density of TiO. We noticed that in the gas phase, Ti is mainly in TiO for temperatures above 1400 K, and TiO_2 dominates at lower temperatures.

Note that Ti chemistry is not enabled by default. Tests show that our linear algebra package can have convergence problems under some extreme conditions when TiO is included. To activate the chemistry, use the command set chemistry TiO on.

3.4. Phosphorous bearing molecules

Phosphorus (P) is essential for the formation of complex compounds, including DNA and RNA, which are fundamental to life. P-bearing molecules have been observed in the Milky Way (Rivilla et al., 2022, 2020; Fontani et al., 2019; Chantzos et al., 2020), as well as in extragalactic environments (Haasler et al., 2022). We have updated the gas-phase chemical reaction rates and molecular lines for P-bearing molecules in the spectral synthesis code CLOUDY. The corresponding molecular reaction rates were obtained from the UDfA. As a result, we predict column densities of 14 P-bearing molecules, PH, PH⁺, PH₂, PH⁺₂, PH₃, PH⁺₃, CP, CP⁺, HCP, HCP⁺, PN, PN⁺, PO, PO⁺. Among these, we predicted molecular lines for PN, PO⁺, and PH₃. Energy levels and radiative and collisional rates for PO, PN, PO⁺, and PH₃ from the LAMDA database.

4. CLOUDY for microcalorimeter X-ray Astronomy

4.1. One-electron Lyman Doublets

With the advent of X-ray microcalorimeters with spectral resolution $R \equiv E/\Delta E > 1200$ at 5.9 keV, such as the one on XRISM, X-ray observations can now resolve the fine-structure doublets of Ly α lines of one-electron species for the first time in astrophysical plasmas (for the Sun, this doublet was already resolved prior to XRISM). Although CLOUDY was not originally designed for high-resolution X-ray spectroscopy, the work in Gunasekera et al. (2024) expanded CLOUDY's treatment of one-electron systems to resolve the H-like Ly α doublets. Earlier work expanded on the two-electron system (Chakraborty et al., 2020a,b, 2021, 2022), included in the C23 release (Chatzikos et al., 2023).

Figure 4, taken from Gunasekera et al. (2024), presents a model of the Perseus cluster core. This model is a collisionally ionized plasma at $T_e = 4.7 \times 10^7$ K, and $n_{\rm H} = 10^{-1.5}$ cm⁻³. The goal here was to resolve the single $np \rightarrow 1s$ lines predicted by CLOUDY, into their fine-structure j-resolved doublets, $np_{1/2} \rightarrow$ $1s_{1/2}$ and $np_{3/2} \rightarrow 1s_{1/2}$. This increases the X-ray spectral resolution of Cloudy to match that of XRISM. Part of the challenge was to retrofit the H-like fine-structure doublets into CLOUDY's already existing full collisional radiative model (hereafter, CRM) solver. Previously, CLOUDY used pseudo-states to represent closely spaced Rydberg levels at high principal quantum numbers (Ferland et al., 2017) to reproduce the classical case B intensities of H and He recombination lines. The pseudo-states were replaced with models of higher-n shells as computers became faster. CLOUDY now employs nl-resolved states for low n, and "Collapsed states" that are not l-resolved for high n.

The "extra" Lyman line arrays in CLOUDY have been expanded to include the treatment of j-resolved Lyman lines of one-electron species, in addition to their original purpose. We left the framework of the He-like "extra" Lyman lines unchanged. We begin by calculating the one-electron np energies, as described by Gunasekera et al. (2024). We then approximate the j-resolved population densities of these lines to the ratio of their statistical weights,

$$n_{npj} = \begin{cases} n_n \left(\frac{g_{np}}{2n^2} \frac{g_{npj}}{g_{np1/2} + g_{np3/2}} \right), & \text{collapsed states} \\ n_{np} \left(\frac{g_{npj}}{g_{np1/2} + g_{np3/2}} \right), & \text{resolved states} \end{cases}$$
 (2)

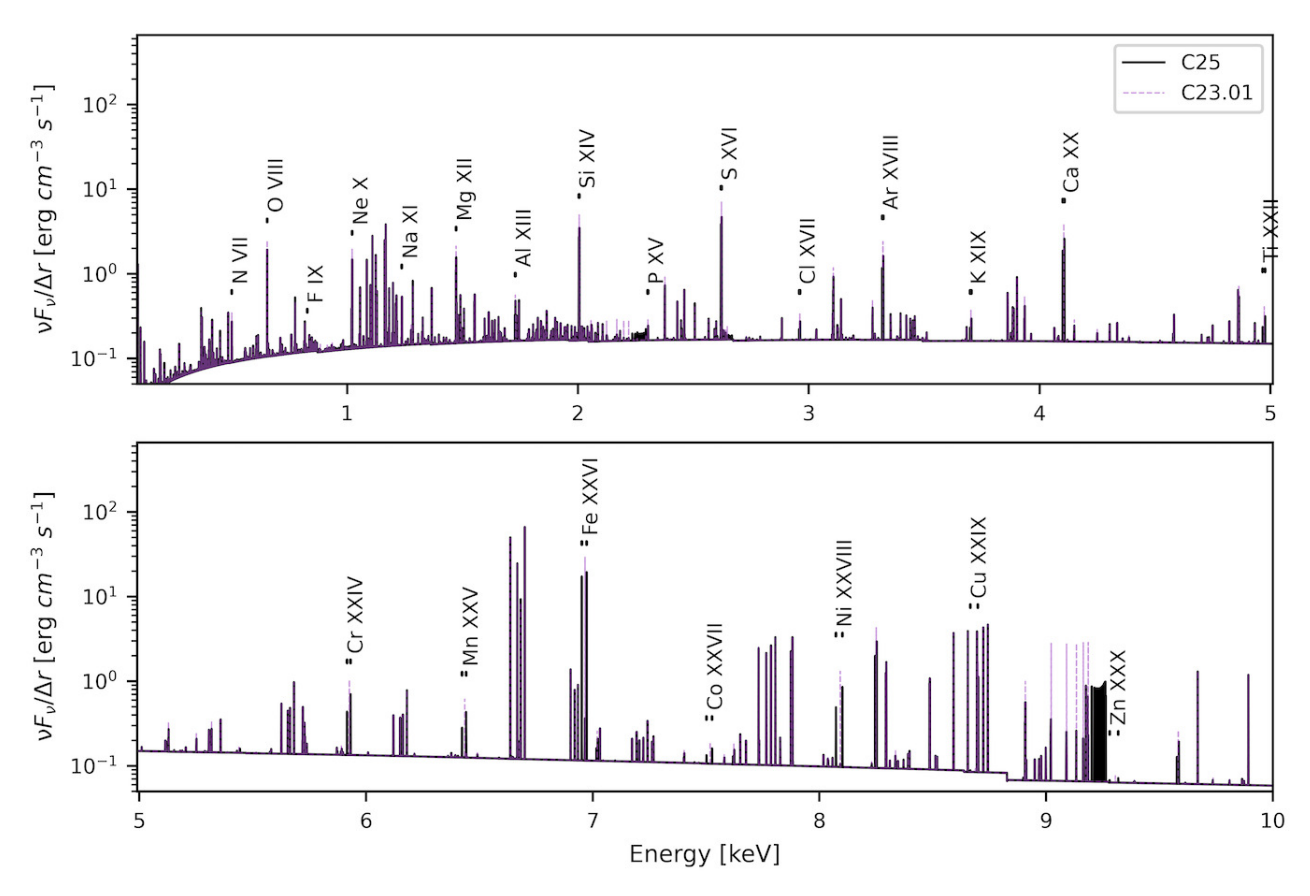


Figure 4. Taken from Gunasekera et al. (2024), CLOUDY simulated spectrum of the Perseus cluster core, showing the j-resolved Lyman α lines in C25. Only the energy range, 0.4 - 10 keV, is covered by the XRISM mission.

where g_i is the statistical weight of level i. Ideally, we can derive their population densities using the CRM solver. The lack of reliable proton-impact j-changing collisional data for most one-electron species makes the aforementioned approximation the best presently available solution.

At the default CLOUDY spectral resolution (further details in 4.1.1), a few low-Z (Z < 8) Ly α_1 and Ly α_2 lines overlap. Figure 5 shows line opacities as a function of line-of-sight velocity for the *j*-resolved Lyman α doublets. Evaluated at temperatures where the ion is most abundant in collisional ionization equilibrium, the figure illustrates how the doublet splitting increases with increasing atomic number (Z). By default, we report the total line intensity for first- and second-row elements, as well as the individual members of the multiple for heavier elements. It is only for the third row and heavier elements that the lines become two non-overlapping lines at the default spectral resolution. For H-like Ly α lines the code uses the theory in Hummer & Kunasz (1980) to calculate the escape probability β , using the line opacities from the coarse continuum. CLOUDY computes nebular spectra using multi-grid methods with two continua: a coarse continuum for overall radiation and continuous processes, and a fine continuum for detailed line transfer and line overlapping (further detail on the fine and coarse continua are given in Shaw et al., 2005). This theory implicitly assumes a single line with a Voigt profile. We updated CLOUDY's escape probability to use the fine opacity mesh instead, which allows for the treatment of overlapping lines (further detailed in Gunasekera et al., 2024). As a result of this update, we no longer allow users to disable the calculation of the fine mesh, and the no $\,$ fine $\,$ opacities command has been removed from the code.

Gunasekera et al. (2025) found that the work described above yielded a novel result: at hydrogen column densities, N(H), above 10^{22} cm⁻² of the X-ray emitting gas, the ratio of the $Ly\alpha_1$ to $Ly\alpha_2$ ratio deviates from the expected 2:1 ratio in the optically thin limit (Tanaka, 1986). Higher column densities correspond to greater optical depths. Therefore, this deviation arises from changes in the optical depths of the j-resolved components of $Ly\alpha$, which reflect the hydrogen column density of the associated gas. Further details on this physics, the above work, and novel N(H) diagnostics are described in Gunasekera et al. (2025) and Gunasekera et al. (2024).

4.1.1. H-like Lyman Resolution Command

The well-known quantum mechanical theory gives us that the fine-structure splitting, that is, the difference between the energy levels $np(^2P_{1/2})$ and $np(^2P_{3/2})$, is of the order $Z^2(n-1)/n^2$ (Bethe & Salpeter, 1957). Therefore, we need to increase the resolving power to resolve the fine-structure lines with increasing n and decreasing Z. The current (XRISM) and future (NewAthena) planned microcalorimeter observatories have spectral resolutions R of 5 eV and 2.5 eV, respectively. Therefore, by default, we set CLOUDY's one-electron fine-structure line spectral resolution to 2.5 eV /10 = 0.25 eV. Consequently, we introduce a new command allowing the user to alter this default resolution, Database H-like Lyman extra resolution R, where R = 0.25 eV by default. Note that we do not allow H and He Lyman lines to be resolved into their fine-structure doublets regardless of the user-set resolution for two important reasons: a) this will

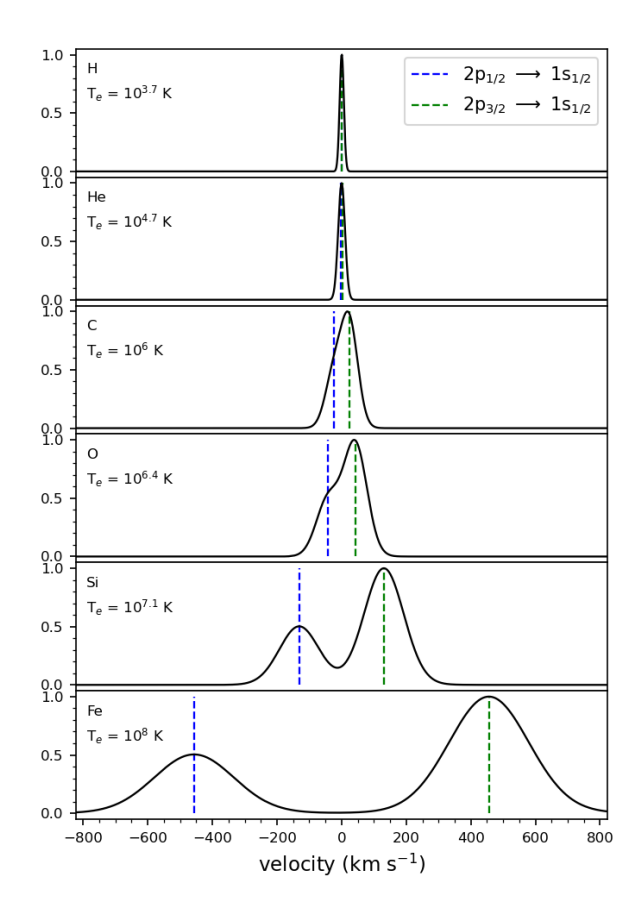


Figure 5. Taken from Gunasekera et al. (2024), this plot shows normalized line opacities against line-of-sight velocity for various one-electron 2p fine-structure doublets at a spectral resolution of 0.25 eV. The blue and green dashed lines mark the positions of the $\mathrm{Ly}\alpha_{j=1/2}$ and $\mathrm{Ly}\alpha_{j=3/2}$ components. The top left corner of each panel indicates the gas temperature, which was chosen to match the peak abundance of the ion under collisional equilibrium conditions. As nuclear mass increases, the line profiles generally become narrower, while higher temperatures cause them to broaden.

break important physics needed by the CLOUDY solvers, and b) current and future known instruments will not be able to resolve these lines.

4.2. Physics of the 1 keV blend

4.2.1. Introducing "mixed" command

Until the previous version, CLOUDY used experimental energy values from the Chianti database by default because of their superior accuracy (Lykins et al., 2013). In the current version, theoretical energy values can now be incorporated in cases where experimental data are absent. The CLOUDY command to use such a "mixed" case is: database Chianti mixed, which was introduced in Chakraborty et al. (2024) and used to explain the origin of the 1 keV feature in X-ray binaries (XRBs).

4.2.2. 1 keV Line Blend

In several instances, spectrometers measure the integrated flux over a defined energy range, which often prevents the unambiguous identification of individual line contributions within the blended spectral features. The Blnd command in CLOUDY, first introduced in Ferland et al. (2017), reports the total flux from the 1 keV line blend, matching what is observed.

A well-known case is the "1 keV feature" in XRBs, where residuals frequently appear between 0.5 and 2 keV owing to unresolved line blends that vary in both centroid and intensity across various types of X-ray binaries as well as over time within the same binary (Paul et al., 2002; Stobbart et al., 2006; Middleton et al., 2015; Walton et al., 2020). Despite numerous modeling efforts using a range of physical scenarios, a comprehensive scientific explanation for the origin and variability of the 1 keV feature remained elusive.

Chakraborty et al. (2024) used the set blend command to construct a line blend using all the lines within the energy range 0.5-2.0 keV. This blend was introduced in blends.ini under the name Blnd 11. The sensitivity of the flux of this line blend was tested against the spectral energy distribution (SED) shape, ionization parameter (ξ), column density ($N_{\rm H}$), and gas temperature (T), following the methodology described in Chakraborty et al. (2020a,b, 2021, 2022) to probe the physical origin and spectral variability of the 1 keV feature.

4.2.3. NewAthena predictions

Using the 1 keV blend, Chakraborty et al. (2024) conducted a thorough analysis of emission and absorption lines under three specific conditions: photoionization equilibrium (PIE), collisional ionization equilibrium (CIE), and reflection of X-rays from the inner regions of an accretion disk. The 1 keV blend was systematically varied with respect to the ionization parameter, temperature, column density, and shape of the SED for five XRBs: two ultraluminous X-ray sources (ULXs), NGC 247 ULX-1 and NGC 1313 X-1; one X-ray pulsar, Hercules X-1; and two low-mass X-ray binaries (LMXBs), Cygnus X-2 and Serpens X-1. The XMM-Newton/RGS and NICER spectra of these sources were fitted using CLOUDY models incorporating the newly implemented 1 keV blend. A self-consistent framework was established to explain the variability of the 1 keV spectral feature, with its diversity attributed to variations in the SED shape, ionization state, temperature, column density, and disk reflection properties.

Figure 6 shows a CLOUDY model of the 1 keV blend in NGC247 ULX-1, based on the SED and best-fit parameters from Chakraborty et al. (2024) at the spectral resolution of the *NewAthena*. This model quantifies the atomic line contributions to the spectrum, including the newly implemented 1 keV line blend in CLOUDY. The spectrum has been decomposed into its individual CIE and PIE components, with strong lines from within the 1 keV blend labeled for clarity.

4.3. Updated Inner Shell Energies

We updated the $K\alpha$ and $K\beta$ fluorescence line energies from the original Kaastra & Mewe (1993) data based on the corrections and prescriptions described in the SRON-SPEX "Atlas of Innershell Ionization lines"¹, which relies on the more accurate data from House (1969) and Bearden & Burr (1967). In particular, we verified that the K-shell transition energies for Fe II to Fe XXII are now in good agreement with the more recent calculations (Palmeri et al., 2003; Mendoza et al., 2004; Bautista et al., 2004). For S and Si, the values remain based on experimental data, as introduced in the patch by Camilloni et al. (2021).

4.4. XRISM/Resolve-specific Initialization File

X-ray microcalorimetry presents unique challenges and opportunities. With the launch of XRISM (Tashiro et al., 2025), these spectra have become a reality in recent years. The CLOUDY team participated in an XRISM-focused CLOUDY workshop in

https://var.sron.nl/SPEX-doc/physics/trpb04c.pdf

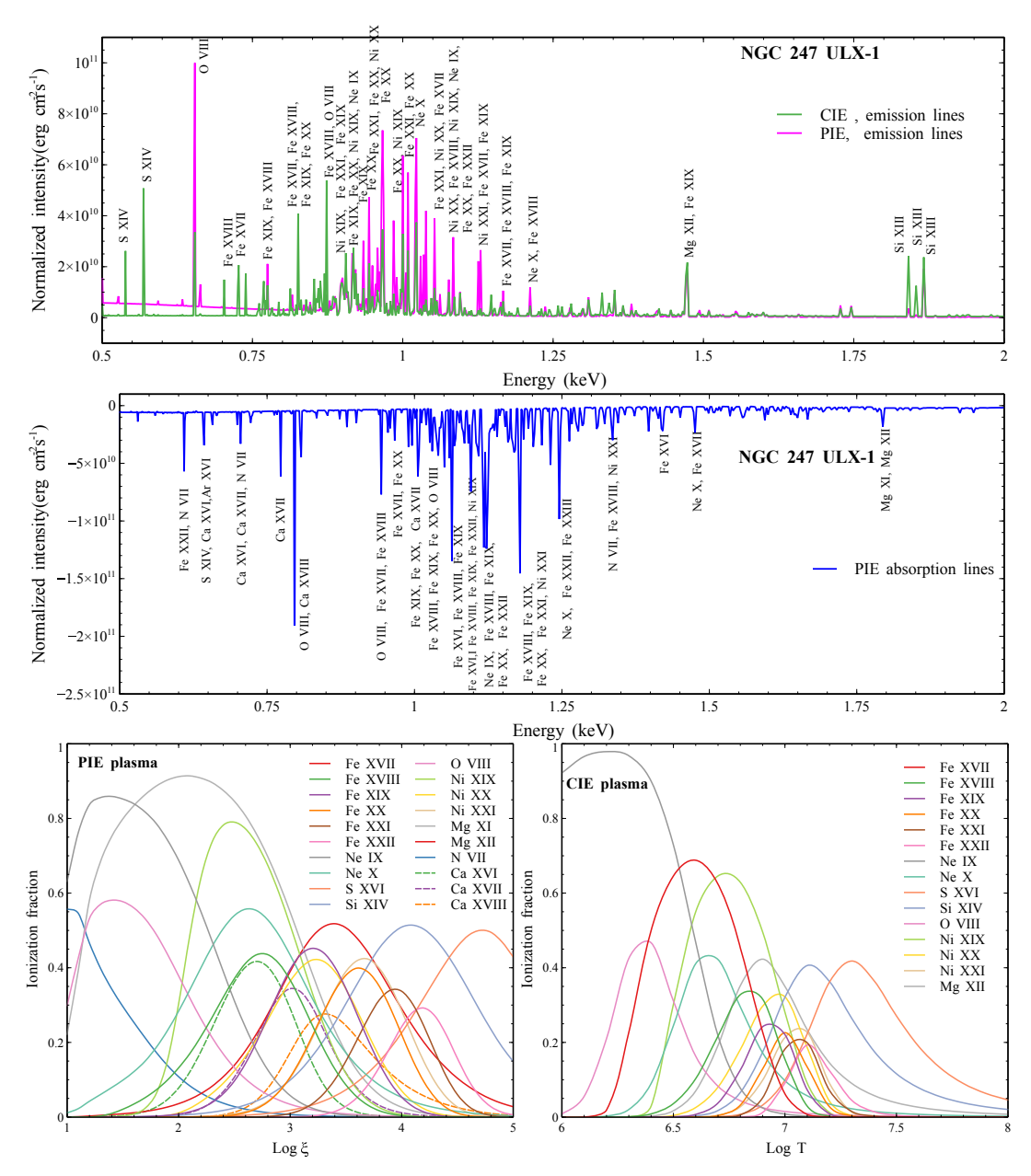


Figure 6. High-resolution CLOUDY model of the 1 keV feature for NGC 247 ULX-1 at the spectral resolution of *NewAthena*. Top panel: Photoionized (PIE) and collisionally ionized (CIE) emission lines at the best-fit values reported in Chakraborty et al. (2024). Middle panel: PIE absorption lines based on the same best-fit model. Bottom left: Charge state distribution of the PIE plasma. Bottom right: Charge state distribution of the CIE plasma. Note that the ionization parameter ξ has a dimension of (erg cm s⁻¹) and is related to the dimensionless U by an additive constant that depends on the shape of the incident SED ($\log(\xi) = \log(U) + const.$).

Tokyo in the Summer of 2024. Several dozen JAXA scientists and students exercised a pre-release version of the code. The team worked to improve the code and obtained interesting results (Gunasekera et al., 2025; Tsujimoto et al., 2025).

The spectral requirements of X-ray microcalorimeters are unique. We added an instrumentation-specific initialization file, XRISM.ini, to the distribution data directory. It increases the continuum spectral resolution and increases the number of levels included in models of 11– through 1–electron iron. The predictions for a simulation of the Perseus cluster are shown in Figure 7.

The higher-fidelity simulation took 50% longer than the simulation with the default state. Its higher spectral resolution is

evident, as is the far larger number of lines. The insights resulting from the microcalorimeter revolution are obvious.

4.5. Updated Fe K Blends

Until the C23.01 release, CLOUDY included Fe K lines heavily utilized by the X-ray community. With this release, the FeK1 and FeK2 lines, which were the one-electron and two-electron K α lines, have been replaced by "Blnd" 1.77982 and "Fe25" 1.85040A respectively. The former is now defined as a blend of the following three lines:

"Fe26" 1.77802A

"Fe26 M1" 1.78330A

"Fe26" 1.78344A

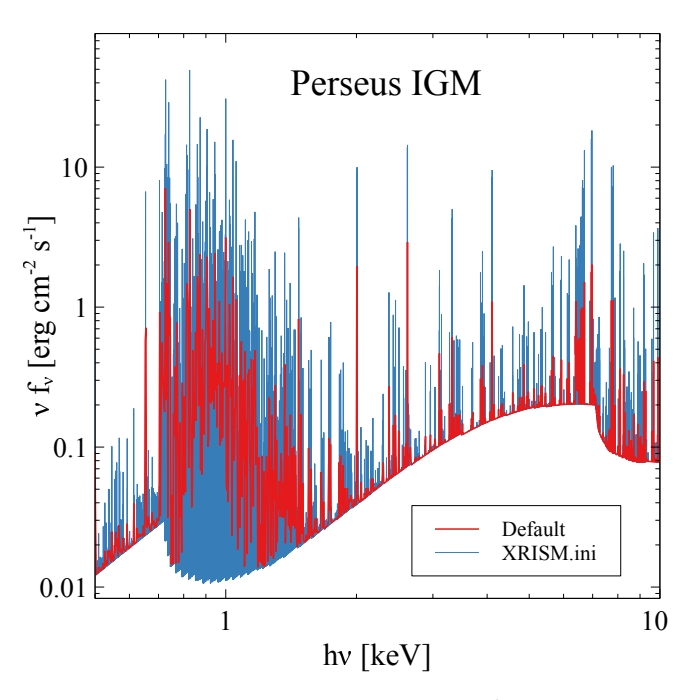


Figure 7. This compares our predicted spectrum of the Perses Cluster cooling flow as modeled by Chakraborty et al. (2020a). It is the same simulation but compares our default setup with the use of our XRISM.ini initialization file.

Additionally, we have removed the following Fe K lines: "FeKH" which were fluorescent hot iron lines from Fe XVIII-Fe XXIII, "FeKC" which were fluorescent hot iron lines from Fe XVII as these are relics from early X-ray astronomy and are no longer relevant in modern studies. Finally, no changes were made to "FeKG", the grain production component of cold Fe.

5. Miscellaneous improvements

5.1. H Ly α escape and destruction probability

In the C23.01 release, we revised our calculation of the H Ly α destruction probability. For details on the updated escape and destruction probability treatment — denoted as $\beta_{\rm HK}$ — see Gunasekera et al. (2023b). As this sub-release was not accompanied by a full review paper, we take this opportunity to outline the resulting changes to the H Ly α physics, which remain relevant in the current release, C25.00.

This updated treatment led to noticeable changes in grain emission, particularly that associated with H Ly α absorption by grains. Figure 8 presents contour plots of the ratio of physical parameters predicted by C23.01 to those from C23.00 using a benchmark H II region model. The three panels show the H Ly α line intensity (left), grain heating from Ly α photon destruction (middle; hereafter "GraL"), and total grain heating from all sources (right).

Dust grains are the main opacity source that absorbs and destroys Ly α photons in H II regions (Spitzer, 1978). With the updated $\beta_{\rm HK}$, more Ly α photons now escape, This reduces the fraction absorbed by dust, thereby lowering grain heating from Ly α destruction (middle panel). Grains are heated by three main mechanisms: (i) the incident radiation field, (ii) collisions with gas particles, and (iii) absorption of line photons such as Ly α . The total grain emission (right panel), reflects the combined effects

of all three, and is reduced slightly owing to the decreased ${\rm Ly}\alpha$ absorption.

However, the total grain emission changes less dramatically than the grain heating by H Ly α because other processes, especially incident starlight, also contribute. Thus, the effects on grain emissions are more subtle. Even in H II regions with moderate dust optical depths, dust can significantly hinder the escape of Ly α photons (Draine, 2011).

The impact of the reduced Ly α destruction is most pronounced at low ionization parameters (U), defined as the ratio of the ionizing photon flux $\phi(H)$ to the hydrogen density n(H). Therefore, in the figure, high U corresponds to the lower-right corner of the panels, and low U corresponds to the upper-left. Bottorff et al. (1998) demonstrated that grain absorption depends on U. At low U, enhanced opacity in the $1s \rightarrow 2p$ transition increases the probability that a Ly α photon is absorbed near its point of origin (a rate referred to as "on-the-spot"; hereafter OTS rate). Because GraL is directly proportional to the OTS rate, the revised destruction probability leads to a significant reduction in both the OTS rate and GraL, particularly at low U.

We find a local minimum of the total grain emission that occurs at $\frac{\phi(H)}{n(H)} \sim 10^{7.2}$ photons cm s⁻¹ (right panel). This arises largely due to the fact that both diffuse field heating and gas-grain collisional heating reach local minima in their relative deviations under the new $\beta_{\rm HK}$ prescription. These "dips" compound the overall reduction in the grain heating efficiency in the low U regime.

Despite these changes to Ly α and grain physics, the new $\beta_{\rm HK}$ has little effect on most of the other observable emission lines. In particular, the classical BPT spectral lines, [O III] λ 5007, [N II] λ 6583, [S II] $\lambda\lambda$ 6716,6731, and [O I] λ 6300 are minimally affected.

5.2. Numerical Methods

A version of the GTH Algorithm (Grassmann et al., 1985; Zhao, 2020), which guarantees the positivity of equilibrium solutions of Markov chains by a specific ordering of operations in Gaussian elimination, has been applied to the atomic level solver in cases where there are no outside sources from other ionization states, or chemical processes. This has addressed an infrequent, but longstanding, code failure mode where negative level abundances were predicted in species such as CaI, and has in general been found to give more accurate results for levels with trace populations.

The dynamical solver has been updated to gracefully handle temperature floors reached in cooling calculations of a recombining gas. Temperature floors may be reached by a gas exposed to intense photoionization, e.g., in the vicinity of a quasar (Reefe et al., 2025), or by an extremely rarefied gas exposed to intense cosmic radiation. In both cases, the externally deposited energy forces the gas to come to equilibrium at a certain temperature, and may prevent it from reaching the temperature prescribed with the stop time when temperature below command. Previously, the solver would continue integrating the evolution of the system to unphysical time-spans, or it could even crash.

5.3. Physical constants

The physical constants have been updated to the Codata 2022 values (Mohr et al., 2024). These changes are very small (typically in the 8th or 9th decimal place) and are unlikely to have a

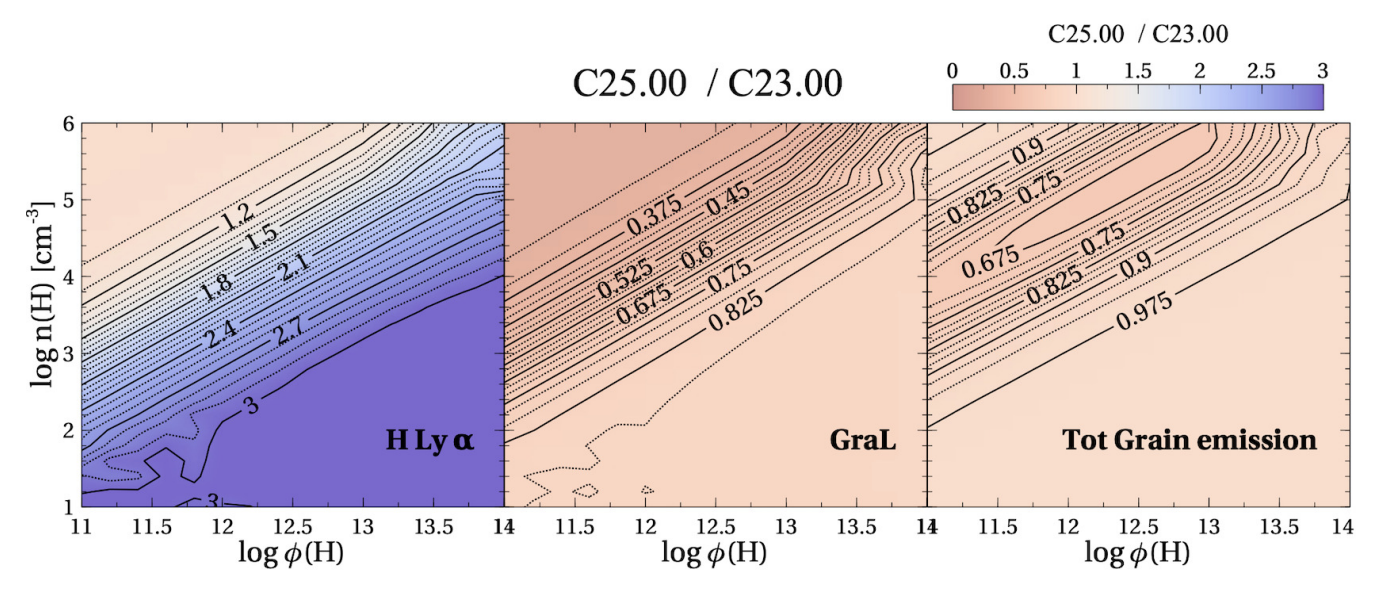


Figure 8. A contour plot of physical parameters predicted by C23.01 relative to the same quantity from C23.00, for the baseline model orion_hii_open.in in the CLOUDY test suite. The panels give, *Left:* taken from Gunasekera et al. (2023b) shows H Ly α , *Middle:* grain heating due to Ly α destruction, *Right:* total grain heating by all sources, lines, collisions, and incident continuum. The ratio of ionizing photon flux $\phi(H)$ to hydrogen density n(H) is effectively the ionization parameter U. The lower-right corner of the panels corresponds to a high U, and the upper-left corner corresponds to a low U.

significant impact on the model. We also changed the value of the solar mass constant from 1.98848×10^{33} g to 1.98841×10^{33} g¹.

6. Infrastructure Changes

6.1. The C++ standard

The language standard used by CLOUDY has changed from C++11 to C++17. This changes the minimum requirements for the supported compilers. For GNU/g++, version 8 or later is required, whereas for LLVM/clang++, version 7 or later is required.

The Oracle Studio compiler has not been maintained for a long time and does not support C++17. Support for this compiler has been discontinued.

6.2. API changes

The API for the routines cdLine() and cdEmis() has been modified. This may affect programs calling CLOUDY as subroutines. When using a wavelength parameter in these calls, it now has to have type t_wavl. This allows the user to indicate whether the wavelength is in air or vacuum.

6.3. Parser changes

The parser now restricts the use of non-ASCII characters in the scripts. They are forbidden in the command part but are still allowed in comments. The code now aborts if they are found where they do not belong. Before this change, the parser would simply skip non-ASCII characters, which could lead to obscure errors. One example is when the number -4 is typed with the Unicode math minus symbol. The Unicode minus symbol would be skipped, and the number would be read as 4 rather than -4.

6.4. Changed commands or options

CLOUDY C22 introduced line disambiguation (Chatzikos et al., 2023). At that time two commands were overlooked: the normalize and stop line commands. Support for line disambiguation has been added to these two commands.

The print line vacuum command was fixed. Following this fix, several changes have been implemented to allow better handling of air and vacuum wavelengths. First, the code now always uses vacuum wavelengths internally and only converts to air wavelengths right before the numbers are printed (this was not the case in older versions of CLOUDY). The conversion will only be done for spectroscopic lines and not for continuum wavelengths (e.g., the save continuum output will always use vacuum wavelengths if wavelength units are requested; this behavior is not new). Several commands have now been amended to allow optional keywords air or vacuum to indicate the wavelength type. This forces the interpretation of the number, regardless of whether the print line vacuum command was used or not. Everywhere line disambiguation is supported, and these new keywords are also supported. Additionally the following commands now accept these keywords: set blend (for the wavelength of the blend itself as well as the components of the blend), print line sort wavelength range, and monitor Case B range (for the wavelength range).

The print path command has been improved. It now accepts an optional string between double quotes, which will be used as a wildcard pattern to match specific data files. Note that the standard C++ ECMAScript grammar for regular expressions will be used, *not* the familiar wildcard characters that most UNIX shells use. This command immediately exits, making it more convenient to find data files.

The table star available command now detects all SED grids, including user-defined grids. The output of this command was completely redesigned. The compile stars command (without additional options) will now also work on user-defined grids.

The keyword quiet for the set blend command has been improved and will quietly ignore the blend if any of the blend components cannot be found.

The illumination command has not changed, but its description in HAZY was incomplete. This description has now

¹https://pdg.lbl.gov/2021/reviews/rpp2021-rev-astrophysical-constants.pdf

been amended. Note that in previous versions of HAZY, the command was sometimes incorrectly called the illuminate command.

The database H-like levels large command now sets a minimum of 160 collapsed levels (10 in previous versions).

The stop time <value> command has been added to allow integration of time-dependent simulations for a preset total amount of time, e.g., 20 Myr. This functionality was used in a recent paper on the mid-infrared emission in the Phoenix galaxy cluster (Reefe et al., 2025). It should also be useful to hydrodynamic simulations that employ CLOUDY as a sub-grid process, or in post-processing of the simulation snapshots.

The following new commands have been added: table SED available, abundances available, and grains available, with functionality similar to the table star available command. To enable Ti-chemistry, the set chemistry TiO on command was added. In addition, the following commands were added to monitor the behavior of the code: monitor itrmax, monitor chemistry steps, monitor chemistry searches, and monitor time elapsed.

The following commands were removed: set numerical derivatives, no fine opacities, and set H2 fraction.

6.5. Other changes

6.5.1. Additional Solar Abundance File

CLOUDY includes a wide variety of solar system elemental abundance tables in its <code>data/abundances/</code> directory, which have been compiled from the literature. Among these are the widely used solar abundance compilations from Lodders et al. (2009) and Lodders (2003), both of which provide recommended values for a complete set of chemical compositions of the solar system. For this particular release of <code>CLOUDY</code>, we have included a new file, <code>data/abundances/Lodders25.abn</code>. This file contains the latest solar abundance recommendations published by Lodders et al. (2025). This new dataset incorporates revised and updated solar photospheric abundances, which recover a higher solar system metallicity. This new abundance set is included as an additional option to replace our default solar composition, which remains unchanged.

6.5.2. Updated Fe II continuum bands

In the file FeII_bands.ini, it was stated that the lower and upper band edges would be treated as vacuum wavelengths. This was not quite how it worked, as the vacuum band edges would be compared to the air wavelengths of the lines in the standard setup. This was fixed, resulting in changes in the predictions for all the continuum bands. In particular, the Fe 2b 4971 and 7785 Å bands are strongly affected by this fix, and a comparison with the results from older CLOUDY versions is not meaningful.

The files FeII_bands.ini and continuum_bands.ini have been renamed to FeII_bands.dat and continuum_bands.dat, respectively, because they are not CLOUDY init files.

6.5.3. New SED files

We added spectral energy distributions (SEDs) for NGC 5548 in both its obscured and unobscured states, based on the multiwavelength modeling presented by Mehdipour et al. (2015). These SEDs are now included in the CLOUDY data directory and can be used to model photoionized regions under realistic AGN conditions. The obscured SED represents the source during its 2013 absorption event, whereas the unobscured version corresponds to its historical unobscured state. Similarly, two new SEDs, obscured and unobscured, were added for Mrk 817.

Both of these SEDs are explained and used in Kara et al. (2021); Dehghanian et al. (2024)

6.5.4. New scripts

To support ongoing STOUT updates and ensure compatibility with the latest NIST Atomic Spectra Database, we revised the NistExtractor.py script available in cloudy/scripts/NistExtractor. The updated version now interfaces with the current NIST API and retrieves up-to-date atomic data. It also supports a broader range of ion name formats (e.g., O_III, o_iii, o_3), which are correctly interpreted as O²⁺. The script outputs a STOUT- compatible directory structure, including .nrg, .tp, and .coll files. Because NIST does not provide collision strengths, the .coll file is left empty.

To retrieve data from NASA ADS and track CLOUDY's citations by version and year, a new script was added to cloudy/scripts/citation-plot. Running this script requires a personal ADS-API-TOKEN. A version of the generated citation plot is updated weekly on CLOUDY's wiki page¹.

7. Cloudy on the Web

CLOUDY is supported by a variety of online platforms that provide users with access to code, documentation, training resources, and published results. The development team maintains these web-based resources to ensure the community has the tools and information needed to run, understand, and properly cite CLOUDY simulations:

- CLOUDY is supported by a robust web presence that provides
 access to documentation, data, and source code. The
 official website, nublado.org, hosts installation guides,
 tutorials, atomic data descriptions, and links to recent
 CLOUDY releases. Users can also explore historical and
 current versions of the code and data through our GitLab
 repository, accessible from the website. CLOUDY's main
 developers actively maintains a record of published versions
 on Zenodo, where users can obtain DOI-referenced software
 packages and associated datasets.
- CLOUDY'S YouTube channel² provides tutorials and instructional videos designed to help users effectively run and interpret simulations with the CLOUDY spectral synthesis code. It covers a range of topics, from beginner introductions to advanced modeling techniques, and is regularly updated with new material, serving as a valuable learning resource for the CLOUDY user community.
- CLOUDY's Papers GitLab repository³ is a central location for accessing scripts used in our published papers related to the CLOUDY project. It includes associated figures and scripts used in the publications. This repository is maintained by the CLOUDY development team to ensure transparency, reproducibility, and accessibility of the scientific results.
- CLOUDY has a long history of development, with multiple released versions and their corresponding documentation sets, known as the Hazy manuals. These versions such as C90, C13, and C17 are listed alongside their respective Hazy references in Table 1. While these prior versions remain archived for reproducibility and legacy support, the authors of CLOUDY strongly encourages users to use the most recent version. This ensures access to the most

¹gitlab.nublado.org/cloudy/cloudy/-/wikis/home

²https://www.youtube.com/@Cloudy-Astroph

³gitlab.nublado.org/cloudy/papers

up-to-date atomic data, physical processes and bug fixes. Accordingly, users should cite the latest CLOUDY release and Hazy documentation to reflect the current state of the code and support the ongoing development of the project. A complete citation for the current version of CLOUDY can be obtained by including the command print citation in your input script when running the code. This will print the appropriate reference for citation in your output file.

8. Future Directions

Since its inception in 1978, CLOUDY has undergone significant development with each new release. Its core mission has been to provide the astronomical community with a robust tool for interpreting the light emitted by astrophysical objects in support of both space- and ground-based observatories. The field of astronomy is rapidly evolving, driven by upcoming missions capable of probing the earliest galaxies to the detailed atmospheric composition of exoplanets. Future observatories will offer improved sensitivity and resolution, surveying vast regions of the sky in unprecedented detail, and placing greater demands on the physical accuracy of simulation tools. Continued development of CLOUDY will therefore be essential to support both standalone applications of CLOUDY and its integration with next-generation hydrodynamic and machine learning codes. We outline below the two key areas in CLOUDY development needed to support future science:

- State-of-the-art of general relativistic magnetohydrodynamic codes, are being developed to study multi-timescale, multiwavelength, and multi-messenger astrophysical plasmas. These simulations depend critically on accurate atomic and molecular data within plasma environments, an area where CLOUDY plays a central role. To continue supporting these advanced hydrodynamic codes, the atomic data of Cloudy must be expanded to provide high-fidelity atomic models.
- The search for potential life beyond solar-system has been rapidly growing over the past two decades, advancing from detecting individual extrasolar planets to detailed studies of exoplanet atmospheres and assessing their potential for hosting life. Current missions such as TESS and JWST are providing insights into atmospheric chemistry, and upcoming missions such as the Roman Space Telescope and Habitable Worlds Observatory will directly image exoplanets in search of biosignatures. Major developments must be undertaken to translate CLOUDY's chemical network to simulate spectra from these exoplanet atmospheres.

8.1. Atomic Data

As part of our ongoing effort to improve CLOUDY's atomic database, we plan to extend the same comprehensive framework used for the C-like isoelectronic sequence to other sequences. In particular, upcoming updates will focus on the Li-like, F-like, Ne-like, Ne-like, Mg-like, and O-like isoelectronic sequences within the Stout database. We continue to adopt a hybrid strategy that prioritizes experimentally anchored quantities as well as targeted studies (wherever available) and supplements them with modern theoretical calculations. These enhancements will ensure consistency across ions and improve the accuracy of CLOUDY's predictions across a wider range of astrophysical environments. These additions will also improve the physical treatment of highlying levels, which play a key role in mediating the transition to statistical equilibrium at high densities. These upper levels

become significantly important as they approach the continuum, where the distinction between bound and free states becomes blurred. Properly modeling this regime is essential to capture the continuum-lowering effects and ensure the thermodynamic consistency of the simulations.

8.2. Molecular Data

Currently, only 47 of the 191 molecules included in CLOUDY have associated spectral lines. In the future, we plan to incorporate internal structures for the remaining molecules to enable the prediction of their spectral lines. In addition, we will include higher vibrational and rotational levels in the molecular models to better support JWST observations. These enhancements will enable CLOUDY to accurately simulate non-local thermodynamic equilibrium (non-LTE) conditions, an essential capability for modeling hot exoplanets, where departures from LTE are common.

8.3. Cloudy at high densities

CLOUDY's goal is to provide reliable results for densities ranging from the low-density limit to densities where the system reaches Local Thermodynamic Equilibrium (LTE) or Strict Thermodynamic Equilibrium (STE). This is a challenging task because of the uncertain physics of highly excited states. Shown in Figs 10 and 11, the 2017 CLOUDY release paper (Ferland et al., 2017) details that the models of one and two-electron systems are well behaved at all densities, and level populations reach the appropriate thermodynamic limits at high densities. Figs 17 and 18 of the 2013 release paper (Ferland et al., 2013) show that the chemistry, ionization, and energy exchange go to the proper thermodynamic limits for a broad range of densities. This 2025 CLOUDY release includes a major expansion in the treatment of excited states with the adoption of a large body of atomic data computed with the R-matrix suite of codes (Del Zanna et al., 2025). This improves the physical treatment of the highest levels that mediate the approach to statistical equilibrium.

However, substantial questions remain. The theory of continuum lowering at high densities is the greatest source of uncertainty. Alimohamadi & Ferland (2022) discuss continuum lowering and its effects on the partition function. Section 3 of that paper shows that the three available theories for continuum lowering at high densities disagree by distressing amounts. A proper theory of dense-plasma continuum lowering remains an unsolved grand challenge problem in physics.

Dielectronic recombination is often the dominant process for complex ions (Osterbrock & Ferland, 2006). This occurs through highly excited and autoionizing states that are greatly affected by continuum lowering. Nigel Badnell and co-workers have created a theory for this suppression and provided numerical fits to density-dependent dielectronic recombination suppression factors (Nikolić et al., 2013, 2018; Gorczyca et al., 2014). These results are used by CLOUDY to account for high-density suppression of recombination.

The CLOUDY team participated in two of the "NLTE#" series of meetings (Chung et al., 2013; Piron et al., 2017). These compared predictions of codes designed for dense plasma laboratory experiments. Discussions at these workshops suggested that the leading cause for disagreement between predictions of the various codes was the treatment of continuum lowering upon dielectronic recombination. This remains an uncertainty.

8.4. Grain Depletions

Gunasekera et al. (2022b) and Gunasekera et al. (2023a) introduced a revised elemental depletion scheme in CLOUDY, based on the work in Jenkins (2009). This depletion framework provides a way for users to vary the overall elemental abundances depleted onto grains using a single parameter, F_{\ast} . However, CLOUDY currently treats the computation of depleted gas abundances independently of the elemental abundances locked into dust grains. Although these two components are intrinsically coupled, the code does not enforce self-consistent depletion across both. Efforts are underway to address this limitation, in which the gas-phase and dust-phase abundances are computed in a mutually consistent manner, ensuring conservation of total elemental content.

We would like to thank the anonymous referee for his/her valuable comments and suggestions, which have helped improve the quality of this paper. CMG and GF acknowledge support from NASA (19-ATP19-0188, 22-ADAP22-0139), JWST-AR-0628, JWST-AR-06419, and NSF (1910687). MD acknowledges support from STScI (JWST-AR-06419.001). MC acknowledges support from NSF (1910687), NASA (19-ATP19-0188, 22-ADAP22-0139), and STScI (HST-AR-14556.001-A). GS acknowledges the WOS-A grant from the Department of Science and Technology, India (SR/WOS-A/PM-2/2021).

■ REFERENCES

- Alimohamadi, P., & Ferland, G. J. 2022, PASP, 134, 073001, doi: 10 .1088/1538-3873/ac7664
- Bautista, M. A., Mendoza, C., Kallman, T. R., & Palmeri, P. 2004, A&A, 418, 1171, doi: 10.1051/0004-6361:20034198
- Bearden, J. A., & Burr, A. F. 1967, RvMP, 39, 125, doi: 10.1103/Re vModPhys.39.125
- Bethe, H. A., & Salpeter, E. E. 1957, Quantum Mechanics of Oneand Two-Electron Atoms (Springer Science & Business Media, 2013)
- Bottorff, M., Lamothe, J., Momjian, E., et al. 1998, PASP, 110, 1040, doi: 10.1086/316222
- Camilloni, F., Bianchi, S., Amato, R., Ferland, G., & Grinberg, V. 2021, RNAAS, 5, 149, doi: 10.3847/2515-5172/ac0cff
- Chakraborty, P., Ferland, G., Fabian, A., et al. 2024, arXiv e-prints, arXiv:2407.02360, doi: 10.48550/arXiv.2407.02360
- Chakraborty, P., Ferland, G. J., Chatzikos, M., et al. 2022, ApJ, 935, 70, doi: 10.3847/1538-4357/ac7eb9
- Chakraborty, P., Ferland, G. J., Chatzikos, M., Guzmán, F., & Su, Y. 2020a, ApJ, 901, 68, doi: 10.3847/1538-4357/abaaab
- —. 2020b, ApJ, 901, 69, doi: 10.3847/1538-4357/abaaac
- -.. 2021, ApJ, 912, 26, doi: 10.3847/1538-4357/abed4a
- Chantzos, J., Rivilla, V. M., Vasyunin, A., et al. 2020, A&A, 633, A54, doi: 10.1051/0004-6361/201936531
- Chatzikos, M., Bianchi, S., Camilloni, F., et al. 2023, RMxAA, 59, 327, doi: 10.22201/ia.01851101p.2023.59.02.12
- Chung, H.-K., Bowen, C., Fontes, C. J., Hansen, S. B., & Ralchenko, Y. 2013, HEDP, 9, 645, doi: 10.1016/j.hedp.2013.06.001
- Churchwell, E., Hocking, W. H., Merer, A. J., & Gerry, M. C. L. 1980, AJ, 85, 1382, doi: 10.1086/112810
- Dehghanian, M., Arav, N., Kriss, G. A., et al. 2024, ApJ, 972, 141, doi: 10.3847/1538-4357/ad5ff4
- Del Zanna, G., Dere, K. P., Young, P. R., & Landi, E. 2021, ApJ, 909, 38, doi: 10.3847/1538-4357/abd8ce

Del Zanna, G., Liang, G., Mao, J., & Badnell, N. R. 2025, Atoms, 13, 44, doi: 10.3390/atoms13050044

- Dere, K. P., Del Zanna, G., Young, P. R., & Landi, E. 2023, ApJS, 268, 52, doi: 10.3847/1538-4365/acec79
- Dere, K. P., Landi, E., Mason, H. E., Monsignori Fossi, B. C., & Young, P. R. 1997, A&AS, 125, doi: 10.1051/aas:1997368
- Draine, B. T. 2011, Physics of the Interstellar and Intergalactic Medium (Princeton University Press: Princeton)
- Ferland, G. J. 1991, Hazy, A Brief Introduction to Cloudy 80 (The Ohio State University Internal Report)
- —. 1993, Hazy, A Brief Introduction to Cloudy 84 (University of Kentucky Internal Report)
- —. 1996, Hazy, A Brief Introduction to Cloudy 90 (University of Kentucky Internal Report)
- Ferland, G. J., Korista, K. T., Verner, D. A., et al. 1998, PASP, 110, 761, doi: 10.1086/316190
- Ferland, G. J., Porter, R. L., van Hoof, P. A. M., et al. 2013, RMxAA, 49, 137. https://arxiv.org/abs/1302.4485
- Ferland, G. J., Chatzikos, M., Guzmán, F., et al. 2017, RMxAA, 53, 385. https://arxiv.org/abs/1705.10877
- Fontani, F., Rivilla, V. M., van der Tak, F. F. S., et al. 2019, MNRAS, 489, 4530, doi: 10.1093/mnras/stz2446
- Gorczyca, T. W., Nikolić, D., Korista, K. T., Badnell, N. R., & Ferland, G. J. 2014, in JPhCS, Vol. 488, 062027, doi: 10.108 8/1742-6596/488/6/062027
- Grassmann, W. K., Taksar, M. I., & Heyman, D. P. 1985, OpRes, 33, 1107, doi: 10.1287/opre.33.5.1107
- Gunasekera, C. M., Chatzikos, M., & Ferland, G. J. 2022a, Astro, 1, 255, doi: 10.3390/astronomy1030015
- Gunasekera, C. M., Ji, X., Chatzikos, M., Yan, R., & Ferland, G. 2022b, MNRAS, 512, 2310, doi: 10.1093/mnras/stac022
- —. 2023a, MNRAS, 520, 4345, doi: 10.1093/mnras/stad322
- Gunasekera, C. M., van Hoof, P. A. M., Chatzikos, M., & Ferland, G. J. 2023b, RNAAS, 7, 246, doi: 10.3847/2515-5172/ad0e75
- —. 2024, arXiv e-prints, arXiv:2412.01606, doi: 10.48550/arXiv.2 412.01606
- Gunasekera, C. M., van Hoof, P. A. M., Tsujimoto, M., & Ferland, G. J. 2025, A&A, 694, L13, doi: 10.1051/0004-6361/202453133
- Haasler, D., Rivilla, V. M., Martín, S., et al. 2022, A&A, 659, A158, doi: 10.1051/0004-6361/202142032
- House, L. L. 1969, ApJS, 18, 21, doi: 10.1086/190183
- Hummer, D. G., & Kunasz, P. B. 1980, ApJ, 236, 609, doi: 10.1086/ 157779
- Jenkins, E. B. 2009, ApJ, 700, 1299, doi: 10.1088/0004-637X/700/2/1299
- Kaastra, J. S., & Mewe, R. 1993, A&AS, 97, 443
- Kamiński, T., Gottlieb, C. A., Menten, K. M., et al. 2013, A&A, 551, A113, doi: 10.1051/0004-6361/201220290
- Kara, E., Mehdipour, M., Kriss, G. A., et al. 2021, ApJ, 922, 151, doi: 10.3847/1538-4357/ac2159
- Kramida, A., Ralchenko, Yu.and Reader, J., & NIST ASD Team. 2024, online, doi: https://doi.org/10.18434/T4W30F
- Landi, E., Del Zanna, G., Young, P. R., Dere, K. P., & Mason, H. E. 2012, ApJ, 744, 99, doi: 10.1088/0004-637X/744/2/99
- Lodders, K. 2002, ApJ, 577, 974, doi: 10.1086/342241
- Lodders, K. 2003, ApJ, 591, 1220, doi: 10.1086/375492
- Lodders, K., Bergemann, M., & Palme, H. 2025, SSRv, 221, 23, doi: 10.1007/s11214-025-01146-w
- Lodders, K., Palme, H., & Gail, H.-P. 2009, Landolt Börnstein, 44, doi: 10.1007/978-3-540-88055-4_34

- Lykins, M. L., Ferland, G. J., Porter, R. L., et al. 2013, MNRAS, 429, 3133, doi: 10.1093/mnras/sts570
- Mao, J., Badnell, N. R., & Del Zanna, G. 2020, A&A, 634, A7, doi: 10.1051/0004-6361/201936931
- Mehdipour, M., Kaastra, J. S., Kriss, G. A., et al. 2015, A&A, 575, A22, doi: 10.1051/0004-6361/201425373
- Mendoza, C., Kallman, T. R., Bautista, M. A., & Palmeri, P. 2004, A&A, 414, 377, doi: 10.1051/0004-6361:20031621
- Middleton, M. J., Walton, D. J., Fabian, A., et al. 2015, MNRAS, 454, 3134, doi: 10.1093/mnras/stv2214
- Millar, T. J., Walsh, C., Van de Sande, M., & Markwick, A. J. 2024, A&A, 682, A109, doi: 10.1051/0004-6361/202346908
- Mohr, P., Newell, D., Taylor, B., & Tiesinga, E. 2024, arXiv e-prints, arXiv:2409.03787, doi: 10.48550/arXiv.2409.03787
- Nikolić, D., Gorczyca, T. W., Korista, K. T., Ferland, G. J., & Badnell, N. R. 2013, ApJ, 768, 82, doi: 10.1088/0004-637X/768/1/82
- Nikolić, D., Gorczyca, T. W., Korista, K. T., et al. 2018, ApJS, 237, 41, doi: 10.3847/1538-4365/aad3c5
- Osterbrock, D. E., & Ferland, G. J. 2006, Astrophysics of gaseous nebulae and active galactic nuclei, 2nd. ed. (Sausalito, CA: University Science Books)
- Palmeri, P., Mendoza, C., Kallman, T. R., & Bautista, M. A. 2003, A&A, 403, 1175, doi: 10.1051/0004-6361:20030405
- Paul, B., Nagase, F., Endo, T., et al. 2002, ApJ, 579, 411, doi: 10.1 086/342701
- Piron, R., Gilleron, F., Aglitskiy, Y., et al. 2017, HEDP, 23, 38, doi: 10.1016/j.hedp.2017.02.009
- Reefe, M., McDonald, M., Chatzikos, M., et al. 2025, Natur, 638, 360, doi: 10.1038/s41586-024-08369-x
- Rivilla, V. M., Drozdovskaya, M. N., Altwegg, K., et al. 2020, MNRAS, 492, 1180, doi: 10.1093/mnras/stz3336
- Rivilla, V. M., García De La Concepción, J., Jiménez-Serra, I., et al.

- 2022, FrASS, 9, 829288, doi: 10.3389/fspas.2022.829288
- Röllig, M. 2011, A&A, 530, A9, doi: 10.1051/0004-6361/201014743
 Schöier, F. L., van der Tak, F. F. S., van Dishoeck, E. F., & Black,
 J. H. 2005, A&A, 432, 369, doi: 10.1051/0004-6361:20041729
- Shaw, G., Ferland, G., & Chatzikos, M. 2023a, RNAAS, 7, 153, doi: 10.3847/2515-5172/ace9b5
- -.. 2023b, RNAAS, 7, 45, doi: 10.3847/2515-5172/acc1ea
- Shaw, G., Ferland, G. J., Abel, N. P., Stancil, P. C., & van Hoof, P. A. M. 2005, ApJ, 624, 794, doi: 10.1086/429215
- Shaw, G., Ferland, G. J., & Chatzikos, M. 2022, ApJ, 934, 53, doi: 10 .3847/1538-4357/ac7789
- Shaw, G., Ferland, G. J., Stancil, P., & Porter, R. 2024, RMxAA, 60, 373, doi: 10.48550/arXiv.2407.20972
- Spitzer, L. 1978, Physical processes in the interstellar medium (New York Wiley-Interscience)
- Stobbart, A. M., Roberts, T. P., & Wilms, J. 2006, MNRAS, 368, 397, doi: 10.1111/j.1365-2966.2006.10112.x
- Storey, P. J., Sochi, T., & Badnell, N. R. 2014, MNRAS, 441, 3028, doi: 10.1093/mnras/stu777
- Tanaka, K. 1986, PASJ, 38, 225
- Tashiro, M., Kelley, R., Watanabe, S., et al. 2025, PASJ, doi: 10.1 093/pasj/psaf023
- Tayal, S. S. 2011, ApJS, 195, 12, doi: 10.1088/0067-0049/195/2/12
 Tsai, S.-M., Malik, M., Kitzmann, D., et al. 2021, ApJ, 923, 264, doi: 10.3847/1538-4357/ac29bc
- Tsujimoto, M., Enoto, T., Díaz Trigo, M., et al. 2025, PASJ, doi: 10 .1093/pasj/psaf022
- Walton, D. J., Pinto, C., Nowak, M., et al. 2020, MNRAS, 494, 6012, doi: 10.1093/mnras/staa1129
- Yerokhin, V. A., & Shabaev, V. M. 2015, JPCRD, 44, 033103, doi: 10 .1063/1.4927487
- Zhao, Y. Q. 2020, Mathematical Theory and Applications, 40, 16. http://mta.csu.edu.cn/EN/Y2020/V40/I2/16